Experimental and Theoretical Investigation of the Stability of Pt−3d−Pt(111) Bimetallic Surfaces under Oxygen Environment

Carl A. Menning, Henry H. Hwu,† and Jingguang G. Chen*

Department of Chemical Engineering, Center for Catalytic Science and Technology, University of Delaware, Newark, Delaware 19716

Received: March 18, 2006; In Final Form: May 26, 2006

The stability of the Pt−3d−Pt(111) (3d = Ti, V, Cr, Mn, Fe, Co, or Ni) bimetallic surface structures in the presence of adsorbed oxygen has been investigated by means of density functional theory (DFT). The dissociative binding energies of oxygen on Pt−3d−Pt(111) (i.e., subsurface 3d monolayer) and 3d−Pt−Pt(111) (i.e., surface 3d monolayer) were calculated. All of the Pt−3d−Pt(111) surfaces were found to have weaker oxygen binding energies than pure Pt(111) whereas all of the 3d−Pt−Pt(111) surfaces were found to have stronger oxygen binding energies than pure Pt(111). The total heat of reaction was calculated for the segregation for 3d metal atoms from Pt−3d−Pt(111) to 3d−Pt−Pt(111) when exposed to a half monolayer of oxygen. All of the Pt−3d−Pt(111) subsurface structures were predicted to be thermodynamically unstable with adsorbed oxygen. In addition, the segregation of subsurface Ni and Co to the surfaces of Pt−Ni−Pt(111) and Pt−Co−Pt(111) was investigated experimentally using Auger electron spectroscopy (AES) and high-resolution electron energy loss spectroscopy (HREELS). AES and HREELS confirmed the trend predicted by DFT modeling and showed that both the Pt−Ni−Pt(111) and Pt−Co−Pt(111) surface structures were unstable in the presence of adsorbed oxygen. The activation barrier of the segregation of surbsurface Ni and Co atoms was determined to be 15 ± 2 and 7 ± 1 kcal/mol, respectively. These results are further discussed for their implication in the design and selection of cathode bimetallic electrocatalysts for the oxygen reduction reaction (ORR) in polymer electrode membrane (PEM) fuel cells.

1. Introduction

In recent years, platinum-based alloys have attracted much research attention for their potential application as cathode electrocatalysts in polymer electrode membrane (PEM) type fuel cells. Specifically, electrodes composed of Pt and another 3d transition metal, such as iron,[1−3] nickel,[1,2,4−10] and cobalt,[1,4,5,7,8,10] have been shown to exhibit activity significantly greater than that of pure Pt for the oxygen reduction reaction (ORR). For example, Stamenković and co-workers reported that, while Pt_3Co and Pt_3Ni electrodes showed improvements over pure Pt for the ORR, alternative "Pt-skin" electrodes produced by sputtering and annealing possessed the maximum catalytic enhancement.[5−8] These experimental results were further supported by density functional theory (DFT) calculations from the Mavrikakis group, where the enhanced ORR activity on the "Pt-skin" system was partially attributed to the alleviation of oxygen poisoning by the shift of the surface d-band center away from the Fermi level.[11,12] Our research group has also performed DFT studies examining the trend in the modification of electronic and chemical properties of Pt(111) by subsurface 3d transition metals.[13−15] For all Pt−3d−Pt systems, the surface d-band was broadened and lowered in energy as compared with Pt, resulting in weaker oxygen adsorption energies.[13−15]

While there is a general agreement that the ORR activity can be significantly improved by modifying Pt electrodes with a layer of subsurface 3d metal, the stability of these bimetallic systems remains unclear. Until recently, much of the cathode research has focused on enhancing the ORR activity while few have reported on the stability and durability of Pt-based alloys. Popov and co-workers evaluated both Pt_3Ni[16,17] and Pt_3Co[17] cathodes with an "accelerated durability test." Two key mechanisms were identified for the observed decay in the ORR activity: (1) the dissolution of the 3d metals during the initial stage of the test and (2) particle migration and agglomeration of the Pt catalyst at longer time scales. Additionally, the authors detected the cross-membrane migration of the 3d metals through cross-sectional analysis of the membrane electrode assembly (MEA).[16,17] Yu et al. compared the stability of conventional Pt/C and alloyed Pt/Co/C cathodes in a dynamic fuel cell environment over 2400 potential cycles.[18] The authors observed an initial reduction in cell performance for both electrodes, but the Pt/Co/C alloy was able to sustain the performance for the subsequent cycles. The dissolution of Co, however, was observed throughout the electrochemical tests.[18]

There also exist various surface science studies examining the interaction of oxygen with model Pt−alloy surfaces.[19−25] In particular, low-energy electron diffraction (LEED) studies revealed that alloy surfaces, such as $Pt_{78}Ni_{22}$(111), $Pt_{80}Ni_{20}$(001), $Pt_{80}Co_{20}$(111), and $Pt_{80}Fe_{20}$(111), all exhibited a pure Pt outermost layer with a Pt-depleted layer underneath.[20] In the presence of oxygen, however, Bardi et al. observed the formation of bulklike Co oxides on the surface of both the (100) and (111) faces of $Pt_{80}Co_{20}$.[19,22] An and co-workers used several surface spectroscopies to examine the oxygen-induced segregation and structural changes of the Pt_3Co(110) surface.[23] An also utilized

* To whom correspondence should be addressed. E-mail: jgchen@udel.edu.
† Current address: Air Products and Chemicals, Inc., Corporate Science and Technology Center, 7201 Hamilton Boulevard, Allentown, PA 18195-1501.

10.1021/jp061697z CCC: $33.50
Published on Web 07/18/2006

scanning tunneling microscopy (STM) to verify and further understand the various LEED patterns observed after different degrees of oxygen exposure.[24] The Goddard group modeled and compared the chemisorption of atomic oxygen on Pt(111) and bimetallic Pt/Ni(111), concluding that oxygen was more tightly bound and more localized on Pt/Ni(111) than on pure Pt(111).[25]

Our research group has previously examined the surface reactivity of Ni/Pt(111)[26] and Co/Pt(111)[27] surfaces, using a combination of surface science techniques and DFT modeling.[13−15] In the reactivity studies, it was determined that the unique surface activity on the bimetallic systems was observed only when annealed to 600 K.[26,27] In brief, deposition of a monolayer coverage of Ni and Co on Pt(111) at 300 K produced reactivity similar to those on Ni and Co surfaces. On the other hand, after heating the surfaces to 600 K, probe reactions showed surface activity unlike those on Ni, Co, or Pt(111) surfaces.[26,27] Additional experimental characterization and theoretical studies determined that the differences between the 300 and 600 K bimetallic surfaces were due to diffusion of monolayer Ni or Co into the subsurface region of Pt(111) at 600 K, producing the Pt−Ni−Pt(111) and Pt−Co−Pt(111) surface structures.[13−15] The primary objective of the current paper is to use Pt−Ni−Pt(111) and Pt−Co−Pt(111) as model systems to determine the stability and energetics for the segregation of subsurface 3d metals in the presence of adsorbed oxygen.

In this manuscript, we will first present DFT calculations that demonstrate the energy differences between oxygen on the Pt−3d−Pt subsurface structure and on the 3d−Pt−Pt surface structure. Using high-resolution electron energy loss spectroscopy (HREELS), we then use the onset of the υ(Ni−O) or υ(Co−O) mode to determine the segregation of subsurface Ni or Co from Pt−Ni−Pt(111) or Pt−Co−Pt(111). Auger electron spectroscopy (AES) measurements following the adsorption of oxygen on Pt−Ni−Pt(111) and Pt−Co−Pt(111) surfaces then allow us to estimate the activation barrier for the segregation of subsurface Ni and Co atoms in the presence of oxygen. Finally, these observations will be discussed in terms of a general trend in the stability and ORR activity of Pt−3d bimetallic cathode electrocatalysts.

2. Experimental Section

2.1. Techniques. The two ultrahigh-vacuum (UHV) chambers used in the current study have been described in detail elsewhere.[27,28] The AES measurements were performed in a two-level UHV chamber (base pressure of 1×10^{-10} Torr) equipped with LEED, a mass spectrometer (MS) for temperature-programmed desorption (TPD), and AES.[27] The HREELS measurements were performed in a separate three-level UHV chamber (base pressure of 6×10^{-10} Torr) equipped with AES, MS, and an LK3000 HREELS unit.[28] The HREEL spectra were acquired with a primary beam energy of 6 eV. Angles of incidence and reflection were 60° with respect to the surface normal in the specular direction. Count rates in the elastic peak were typically in the range of 6×10^5 to 2×10^6 counts-per-second (cps), and the spectral resolution was between 25 and 40 cm^{-1} fwhm (full-width at half-maximum). For both AES and HREELS experiments, the single-crystal surface was heated at 3 K/s.

2.2. Surface Preparation. The single-crystal sample was a [111] oriented, 1.5 mm thick, and 8 mm in diameter platinum disk (99.999%). The sample was spot welded directly to two tantalum posts that served as contacts for liquid nitrogen cooling and resistive heating. This mounting scheme permitted the sample temperature to be varied between 80 and 1150 K. The Pt(111) surface was cleaned with Ne^+ sputtering at 500 K and with O_2 treatment at 600 K, followed by annealing at 1100 K. Surface contaminants such as carbon and oxygen were below the detection limits of AES after the above cleaning procedures.

Monolayer coverage of Ni or Co was deposited onto Pt(111) from an evaporative doser, consisting of high-purity Ni or Co wire wrapped around a tungsten filament. The bimetallic structures with surface monolayer of Ni or Co were prepared with the Pt(111) crystal temperature maintained at 300 K; the subsurface Pt−Ni−Pt(111) and Pt−Co−Pt(111) structures were obtained by heating to 600 K based on conditions developed in our previous studies.[13,27]

3. Density Functional Theory (DFT) Calculations

3.1. Methods. The bimetallic surfaces were modeled using a 2×2 unit cell extended to three layers of metal atoms with each layer composing of four metal atoms. This unit cell was expanded using periodic boundary conditions with 4−6 equivalent layers of vacuum separating the slabs to isolate each metal slab. The adsorption of atomic oxygen was modeled on two slab configurations. The first slab was the Pt−3d−Pt subsurface configuration. This configuration was modeled with the first and third layers composed of Pt atoms and the second layer of four atoms substituted with one of the 3d transition metals from Ti to Ni. The alternative configuration was the 3d−Pt−Pt surface configuration, where the 3d transition metal atoms were present on the surface. This was modeled by substituting the first layer of Pt metal atoms with one of the 3d transition metals from Ti to Ni, with the second and third metal layers consisting entirely of Pt atoms. Two of the four face centered cubic (fcc) 3-fold hollow sites for the unit cell were filled with O atoms to simulate a half monolayer coverage of oxygen. The two oxygen atoms and the first metal layer for both configurations were allowed to relax to the lowest energy configuration while the second and third metal layers were held at the bulk Pt−Pt distance of 2.84 Å, which has been determined previously using the RPBE exchange/correlation functional.[29] The energy level was calculated using the DACAPO v2.7 code, which represents the core electrons of each atom with ultrasoft Vanderbilt pseudopotentials and uses plane waves as the basis set.[30] The calculations used a Chadi−Cohen k-point set and a plane wave cutoff of 340 eV.

3.2. Stability of the Pt−3d−Pt Subsurface Structure with Adsorbed Oxygen. DFT calculations with the DACAPO code were used to compare the trend in the binding energy of atomic oxygen on Pt−3d−Pt and 3d−Pt−Pt bimetallic configurations. It has been shown previously that the activity of a cathode electrocatalyst for the oxygen reduction reaction (ORR) can be related to the binding energy of oxygen.[11,12,31] Therefore, the dissociative binding energy for oxygen was calculated for each of the Pt−3d bimetallic systems in both the subsurface and surface configurations. The results of these calculations are shown in Figure 1 as a function of surface d-band center. There is a nearly linear trend in the binding energy of oxygen on the subsurface Pt−3d−Pt structure, with the weakest binding energy on Pt−Ti−Pt and the strongest binding energy on Pt−Ni−Pt. In comparison, all of the Pt−3d−Pt subsurface structures have weaker oxygen binding energies than that on pure Pt(111). For the 3d−Pt−Pt surface configuration, there is again a nearly linear trend in the binding energy with respect to the surface d-band center. However, this trend is opposite to that of the subsurface configuration. For example, the Ti−Pt−Pt surface has the strongest oxygen binding energy while the Ni−Pt−Pt surface has the weakest binding energy. All of the 3d−Pt−Pt

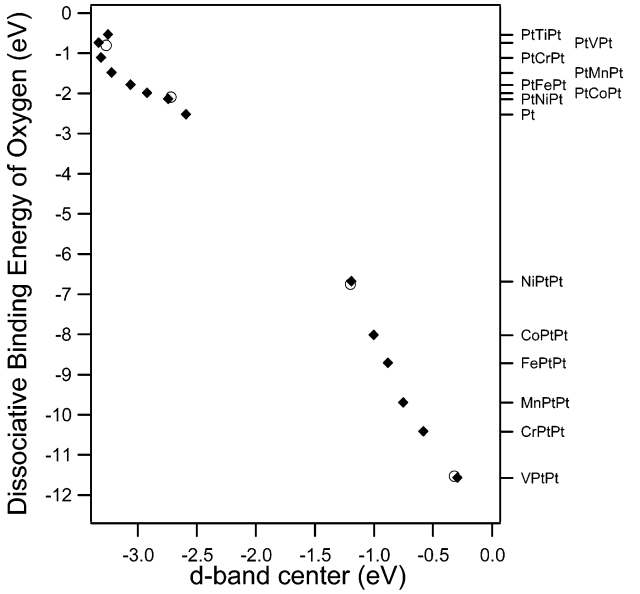

Figure 1. Calculated dissociative binding energy of oxygen on Pt−3d bimetallic surfaces with 0.5 ML oxygen coverage vs surface d-band center.

systems have oxygen binding energies stronger than that on pure Pt(111), suggesting that these bimetallic surfaces should have lower activity toward the ORR than Pt(111) due to the poisoning by the strongly bonded oxygen atoms.

In the DFT results in Figure 1, oxygen atoms and the first metal layer for both configurations were allowed to relax to the lowest energy configuration while the second and third metal layers were held at the bulk Pt−Pt distance. To determine whether this geometry would cause significant changes in oxygen binding energy, we have also performed DFT studies of oxygen on four surfaces, Pt−Ni−Pt(111), Pt−V−Pt(111), Ni−Pt−Pt(111), and V−Pt−Pt(111), with the second layer also allowed to relax. These results are represented as open circles in Figure 1, which shows that the difference in the oxygen binding energy is less than 0.1 eV between the two types of structure models, which should not affect the general trend in Figure 1. Because our primary interest is in the trend, not the absolute values, of binding energies on different surfaces, it is justified to use the slab with the second and third layers fixed to reduce the computation time.

Results from our previous experimental and DFT studies have shown that the Pt−3d−Pt subsurface structure is thermodynamically more stable than the 3d−Pt−Pt configuration under vacuum or with adsorbed atomic hydrogen.[13,27] However, DFT results in Figure 1 indicate that the trend in the relative stability is different in the presence of absorbed oxygen. The stability of the Pt−3d bimetallic systems can be determined by comparing the difference in total energy, ΔE, between the subsurface and surface configurations when exposed to a half monolayer of oxygen. The reaction coordinate for this process is illustrated in Figure 2. The shaded spheres represent the Pt atoms, the spheres with dashed lines represent the 3d transition atoms, and the smaller solid spheres represent the oxygen atoms. The total energy difference should be proportional to the heat of reaction and should allow the prediction of which configuration is thermodynamically favored in the presence of adsorbed oxygen atoms. Figure 3 shows the values of ΔE for the Pt−3d bimetallic surfaces from Ti to Ni. In each case, the 3d−Pt−Pt surface configuration is lower in energy than that of the corresponding subsurface configuration, indicating that the Pt−3d−Pt subsurface structures are thermodynamically unstable with adsorbed

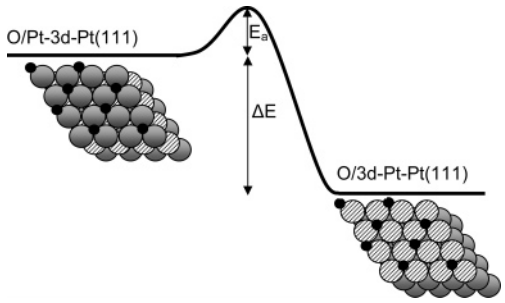

Figure 2. Reaction coordinate for bimetallic stability between the subsurface configuration and surface configuration: gray spheres are Pt, slashed spheres are 3d group transition metal atoms, and the small dark spheres are O atoms.

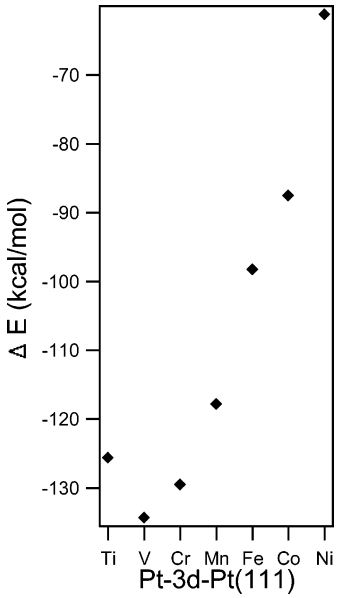

Figure 3. Calculated total energy differences, ΔE, between O/Pt−3d−Pt(111) and O/3d−Pt(111) bimetallic configurations with 0.5 ML oxygen coverage.

oxygen. The remainder of this study will attempt to experimentally quantify the stability of the Pt−3d−Pt subsurface configuration by determining the activation barrier, E_a, for the segregation of subsurface Ni or Co atoms to the surface.

4. Experimental Results

4.1. Preparation of Pt−Ni−Pt and Pt−Co−Pt Subsurface Structures. The surface compositions of Ni/Pt(111) and Co/Pt(111) were monitored by using the Ni(849 eV)/Pt(241 eV) and Co(777 eV)/Pt(241 eV) Auger ratios, respectively. Figure 4 shows the Ni/Pt and Co/Pt AES ratios as a function of annealing temperature, after the deposition of approximately one monolayer Ni or Co on Pt(111) at 300 K. The AES scans for temperatures 300, 350, and 400 K were obtained after holding the surface for 30 s at those temperatures before the AES measurement at these temperatures. For scans at 450 K and above, the surface was first held at the indicated temperatures for 30 s and then cooled to 400 K for recording the AES spectra. This procedure was used to minimize the inward diffusion of Ni or Co atoms during the AES scans (∼5 min per scan) at $T > 400$ K.

Both curves in Figure 4 show that the Auger ratio decreases significantly between 300 and 600 K, indicating the inward diffusion of Ni and Co atoms into Pt(111). The Ni/Pt AES ratio at 300 K is ∼1.64, which decreases to ∼1.13 upon heating to

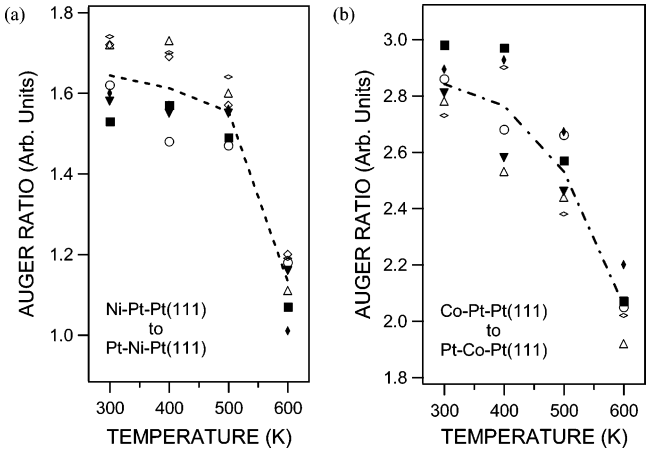

Figure 4. (a) Ni(849 eV)/Pt(241 eV) AES ratios after heating various coverages of Ni on Pt(111) from 300 to 600 K. (b) Co(777 eV)/Pt(241 eV) AES ratios after heating various coverages of Co on Pt(111) from 300 to 600 K.

600 K. Similarly, the Co/Pt AES ratios at 300 and 600 K are ~2.84 and ~2.06, respectively. The starting coverages of Ni and Co on Pt(111) at 300 K were chosen to achieve approximately a one-to-one ratio of Ni/Pt or Co/Pt at the first two atomic layers. After accounting for differences in the inelastic mean free paths of the electrons, atomic radii, and Auger sensitivity factors, our research group had previously estimated the onset of a monolayer at 600 K to be at Auger ratios of Ni(849 eV)/Pt(241 eV) ~1.0 [32] and Co(777 eV)/Pt(241 eV) ~2.0.[27] For the remainder of this paper, we will refer to the freshly deposited Ni/Pt or Co/Pt surfaces at 300 K as the Ni−Pt−Pt(111) or Co−Pt−Pt(111) surface structures and the 600 K surfaces as the Pt−Ni−Pt(111) or Pt−Co−Pt(111) subsurface structures.

4.2. Vibrational Studies of Oxygen on Pt−Ni−Pt(111) and Pt−Co−Pt(111). *4.2.1. Oxygen on Pt−Ni−Pt(111).* HREELS measurements were performed following the adsorption of saturation coverage oxygen on clean Pt(111), a Ni film (>5 ML) on Pt(111), and Pt−Ni−Pt(111). The purpose of these experiments was to identify the characteristic ν(metal−O) frequencies for each surface, which will be used as an indication for the segregation of Ni from Pt−Ni−Pt(111) onto the surface. The exposure of oxygen was made with the crystal temperature at 120 K. The adsorbed layers were then heated to the indicated temperatures and cooled immediately before the HREEL spectra were recorded. The height of the elastic peaks in all spectra was normalized to unity, and the expansion factor for each individual spectrum was the multiplication factor relative to the elastic peak.

The bottom spectrum in Figure 5a shows the adsorption of oxygen on Pt(111), which closely resembles previously reported HREELS measurements.[33,34] In those studies, submonolayer oxygen coverages on Pt(111) showed only one vibrational mode near 470 cm^{-1}, similar to the 467 cm^{-1} feature in the current study. This vibrational mode has been assigned to the ν(Pt−O) mode of atomic oxygen on the fcc 3-fold hollow sites of Pt(111).[35]

The remaining HREEL spectra in Figure 5a were conducted with the aim of identifying the onset temperature for the segregation of Ni atoms from the subsurface to the surface under oxidizing conditions. The spectra were obtained by first exposing 200 L of O_2 to Pt−Ni−Pt(111) at 300 K, then cooled to 110 K before the HREEL spectrum was recorded. The surface was then heated to the next temperature and exposed to another

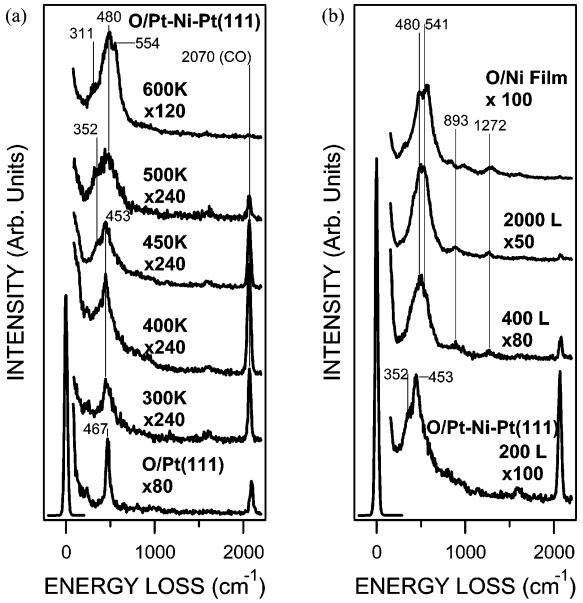

Figure 5. (a) 200 L O_2 adsorption on subsurface Pt−Ni−Pt(111) at various temperatures. The bottom spectrum is 200 L O_2 exposure on clean Pt(111). (b) Various O_2 exposures on Pt−Ni−Pt(111) at 450 K. The top spectrum is after 200 L O_2 exposure on a thick Ni film (>5 ML) deposited on Pt(111).

200 L of O_2 without any surface cleaning. After oxygen exposures at 300 and 400 K, two vibrational features are present at 453 and 2070 cm^{-1}, which are assigned to ν(Pt−O) and ν(CO) (background contamination), respectively. The ν(Pt−O) mode at 453 cm^{-1} is similar to the ν(Pt−O) mode at 467 cm^{-1} on clean Pt(111), suggesting that the first atomic layer is predominantly Pt and that the subsurface structure is stable under oxidizing conditions at 400 K or below. The 450 K spectrum is generally the same as the 300 and 400 K spectra, except the onset of a shoulder peak at ~352 cm^{-1}. The appearance of this peak may be attributed to either the shifting of the adsorbed oxygen to an alternative binding site, or the early-stage segregation of Ni to produce the Ni−O bond. By 500 K, the ν(metal−O) mode is substantially broadened, with the peak center shifting to ~480 cm^{-1}. After oxygen exposure at 600 K, overlapping features can be identified at 311, 480, and 554 cm^{-1}. The spectrum is very similar to that after exposing a thick Ni film (>5 ML) to oxygen (top spectrum in Figure 5b), indicating the segregation the subsurface Ni atoms to the surface at 600 K.

Because 450 K was identified as the onset temperature for the segregation of subsurface Ni in Pt−Ni−Pt(111), additional HREELS experiments were conducted to examine the dependence of Ni segregation on oxygen exposure at 450 K. Figure 5b shows the HREELS measurements following various exposures of O_2 on Pt/Ni/Pt(111) at 450 K. The dominant ν(metal−O) mode shifts from 453 at 200 L to ~480 cm^{-1} at 400 L of O_2 exposure, with a shoulder peak appearing at ~541 cm^{-1}.[36] The ν(metal−O) modes after 2000 L are similar to the 400 L exposure, with a slight increase in peak intensity. Furthermore, the spectrum after 2000 L O_2 exposure is similar to that following the dissociative adsorption of oxygen onto 300 K Ni/Pt(111) (top spectrum in Figure 5b). The features 480 and 541 cm^{-1} have been previously assigned to the ν(Ni−O) modes of two different NiO structures.[36,37] Overall, the HREELS results in Figures 5 indicate that the segregation of subsurface Ni occurs at 450 K or higher, although more quantitative analysis is needed to determine the diffusion kinetics of Ni from the Pt−Ni−Pt(111) subsurface as described later.

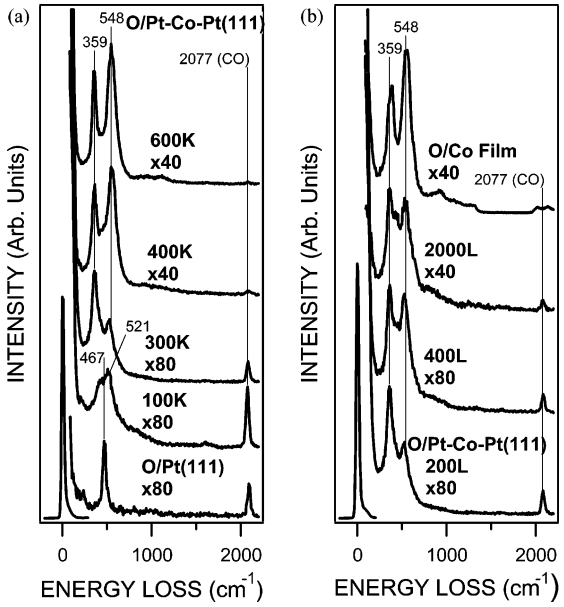

Figure 6. (a) 200 L O_2 adsorption on subsurface Pt−Co−Pt(111) at various temperatures. The bottom spectrum is 200 L O_2 exposure on clean Pt(111). (b) Various O_2 exposures on Pt−Co−Pt(111) at 300 K. The top spectrum is after 200 L O_2 exposure on a thick Co film (>10 ML) deposited on Pt(111).

4.2.2. Oxygen on Pt−Co−Pt(111). Similar HREELS measurements were performed to investigate the segregation of Co from Pt−Co−Pt(111), as shown in Figure 6. Figure 6a demonstrates the effect of exposing Pt−Co−Pt(111) to 200 L O_2 at different temperatures. After exposing the Pt−Co−Pt(111) surface to 200 L O_2 at 100 K, the HREEL spectrum is different from that on clean Pt(111). The 100 K spectrum is characterized by the υ(Pt−O) peak at 467 cm^{-1}. However, even at such a low temperature, a second peak is detected at 521 cm^{-1}, suggesting the presence of additional adsorption sites due to the modification of Pt(111) by Co, even at 100 K. As the temperature is increased to 300 K, the υ(Pt−O) mode disappears and Co−O vibrational modes are detected at 359 and 548 cm^{-1}. As the temperature is increased to 400 and 600 K, the two υ(Co−O) peaks increase in intensity, with the feature at 548 cm^{-1} becoming the dominant peak. These two υ(Co−O) modes are similar to the peaks seen by Schwarz et al., for oxygen on the Co(1010) surface corresponding to a c(2 × 4) phase.[38] Similar to the assignment by Schwarz et al., the υ(Co−O) peak at 548 cm^{-1} is attributed to a vibration perpendicular to the surface and the δ(Co−O) peak at 359 cm^{-1} is attributed to a bending mode parallel to the surface.[38]

The higher segregation rate of the subsurface Co atoms, as compared with the subsurface Ni, is further demonstrated in Figure 6b. The bottom three HREELS spectra were recorded after exposing Pt−Co−Pt(111) to increasing amounts of oxygen at 300 K. The (Co−O) features are already well defined after 200 L O_2 exposure. The spectra after 400 and 2000 L exposures are similar, indicating that the segregation of Co atoms is nearly complete after exposure to 400 L O_2. The top spectrum in Figure 6b is after 200 L of O_2 exposure onto a thick Co film (>10 ML) on Pt(111). This surface also displays the two υ(Co−O) vibrations at the same frequencies as those on Pt−Co−Pt(111) after being exposed to O_2 at 300 K. This further supports the assignment of the vibrations at 359 and 548 cm^{-1} to the (Co−O) modes, indicating the segregation of subsurface Co atoms onto the surface in the presence of oxygen at 300 K.

4.3. Auger Studies of Stability of Pt−Ni−Pt(111) and Pt−Co−Pt(111). *4.3.1. Oxygen on Pt−Ni−Pt(111).* AES measurements were performed to determine the increase in the surface Ni/Pt ratio as a function of oxygen exposure time. These experiments were performed at several temperatures to estimate the activation barrier (E_a) for transforming Pt−Ni−Pt(111) to a Ni−Pt−Pt(111) in the presence of oxygen. These measurements were performed in a different UHV system, with oxygen being delivered through a directional doser placed approximately 3 cm away from the sample. During oxygen dosing, the chamber background pressure was maintained at 5×10^{-8} Torr, which correlates to a rate of O_2 exposure at approximately 0.2 ML/s.

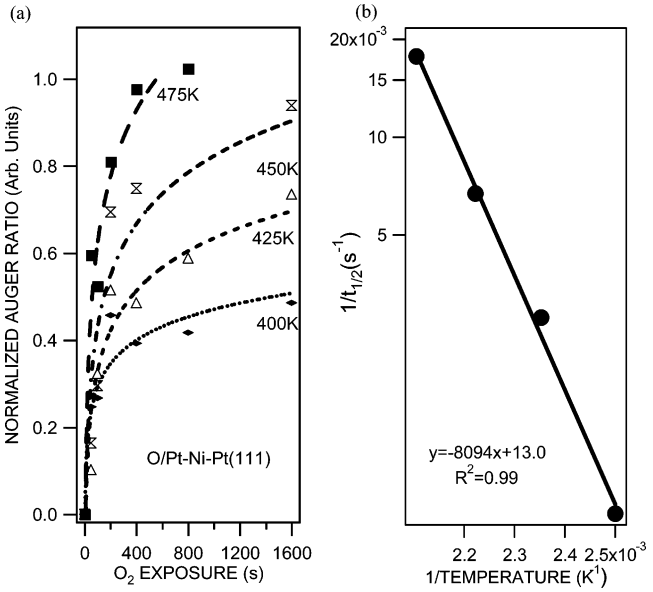

Figure 7. (a) Normalized Ni/Pt Auger ratios at various temperatures and (b) activation barrier from Pt−Ni−Pt(111) to Ni−Pt−Pt(111) in oxygen environment.

Figure 7a shows the Ni/Pt AES ratios as a function of time at various temperatures between 400 and 475 K. The AES ratio is renormalized to where a value of 0 represents only Pt in the first layer (Ni/Pt AES ratio ∼1.0 after heating to 600 K) and 1 represents only Ni in the first layer (Ni/Pt AES ratio ∼1.7 after heating to 600 K). The general equation for temperature-dependent segregation can expressed as

$$k = Ae^{-E_a/RT} = \frac{C}{t_{1/2}} \tag{1}$$

where k is the rate constant, A is the preexponential factor, $t_{1/2}$ is the time required for $^1/_2$ of the subsurface Ni to segregate onto the surface, and C is a time-independent parameter whose value is related to the reaction order of the segregation process. Equation 1 can be rearranged to estimate the value of the apparent activation barrier E_a

$$-\ln(t_{1/2}) = -\frac{E_a}{RT} + \ln\left(\frac{A}{C}\right) \tag{2}$$

Through the use of the best log fit equations to derive an approximate time required to reach 0.5, or $t_{1/2,}$ for each temperature, an ln $1/t_{1/2}$ vs reciprocal temperature plot is generated in Figure 7b. On the basis of the best fit linear equation for data points between 400 and 475 K, the E_a for the segregation of subsurface Ni is estimated to be 15 ± 2 kcal/mol. The error bar is estimated based on results from multiple sets of AES measurements. Results above 475 K were excluded because the competitive inward diffusion of Ni atoms started to occur at this temperature, as shown earlier in Figure 4.

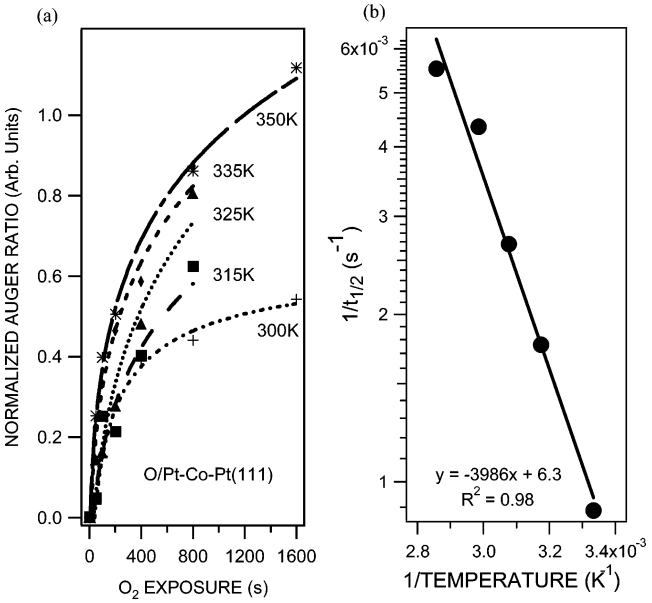

Figure 8. (a) Normalized Co/Pt Auger ratios at various temperatures and (b) activation barrier from Pt−Co−Pt(111) to Co−Pt−Pt(111) in oxygen environment.

4.3.2. Oxygen on Pt−Co−Pt(111). Similar AES measurements were conducted to estimate the E_a value for transforming Pt−Co−Pt(111) to Co−Pt−Pt(111) in the presence of oxygen. Similar to the procedure used for the Ni/Pt(111) experiments, the *y*-axis in Figure 8a is calibrated with values of 1 and 0 being equivalent to Co/Pt Auger ratios of approximately 2.8 (1 ML surface Co at 300 K) and 2.0 (after heating to 600 K), respectively. The initial experiments were performed using the same oxygen exposure rate and temperature regime as that in Figure 7a, which resulted in a very low E_a value of ∼3 kcal/mol for the segregation of subsurface Co to the surface. The low E_a value suggested the possibility that the segregation of Co to the surface occurred at the same time as the diffusion of Co into the subsurface in the temperature range of 400 and 475 K. As a result, additional experiments were performed at lower temperatures to obtain a more accurate estimate of the Co segregation activation barrier. Figure 8 shows the AES measurements and the linear fit for oxygen exposure on Pt−Co−Pt-(111) between 300 and 350 K. Through the use of similar analysis procedures described for Pt−Ni−Pt, the E_a value is estimated to be between 7 ± 1 kcal/mol for the segregation of subsurface Co atoms at the temperature regime of 300−350 K.

5. Discussion

5.1. General Trend in the Stability of Pt−3d Bimetallic Surfaces. Our research group has previously investigated the stability and activity of the Pt−3d−Pt subsurface structures without adsorbates and also in the presence of adsorbed atomic hydrogen.[14,15,26,27,39] From DFT calculations, the Pt−3d−Pt subsurface structures are thermodynamically more stable than the corresponding 3d−Pt−Pt structures in both cases. From the point of view of surface reactivity, the presence of the subsurface 3d layer shifts the center of the surface d-band away from the Fermi level as compared with pure Pt, leading to weakened adsorbate−metal bonds on the Pt−3d−Pt surface. These theoretical predictions have been confirmed experimentally based on hydrogen TPD experiments on the Pt−Ni−Pt and Pt−Co−Pt surfaces.[26,27] The presence of weakly bonded hydrogen led to novel low-temperature hydrogenation pathways, as reported in detail in our previous studies.[14,15,26,27,39]

In the current study, however, our results indicate that the Pt−3d−Pt subsurface structures are not thermodynamically stable in the presence of adsorbed atomic oxygen. The segregation of subsurface Co and Ni to the surface is detected experimentally in the AES and HREELS measurements, consistent with the DFT predictions that the 3d−Pt−Pt surfaces are more stable than Pt−3d−Pt in the presence of oxygen. These conclusions are also consistent with previous studies on Pt−3d bimetallic alloy single crystals.[19,22−24] For example, An's STM studies showed the gradual formation of Co−O clusters from low to higher exposures (5 L) at 773 K.[23,24] XPS and LEIS studies by Bardi and co-workers indicated the formation of oxide islands with oxygen exposures at 600 K, eventually leading to the formation of a surface CoO layer.[23,24] The oxygen-induced segregation has also been previously reported for the Au/Mo/Au(111) subsurface structure due to the formation of Mo oxide.[40]

Although both subsurface Co and Ni atoms segregate to the surface in the presence of oxygen, our results reveal that the onset temperatures for the observed segregation are different. For example, the amount of Co segregation to the surface at 300 K is approximately the same as the amount of Ni segregation at 400 K. This difference is reflected in the apparent activation barrier for segregation for the two bimetallic systems, which is 7 ± 1 kcal/mol for Co and 15 ± 2 kcal/mol for Ni, as determined experimentally in Figures 7 and 8. Furthermore, assuming the magnitude of the activation barrier is related to the difference in the total energy between O/3d−Pt−Pt and O/Pt−3d−Pt, the DFT trend in Figure 3 suggests that the activation barrier for the segregation of other subsurface 3d metals (Ti, V, Cr, Mn, Fe) should be even lower than that for Co or Ni.

The transformation of the Pt−3d−Pt subsurface structure to the 3d−Pt−Pt surface structure has important implications to the activity in the cathode ORR reactions. As pointed out by Mavrikakis et al.,[11] the enhanced ORR reactivity of the Co/Pt alloy surface, as compared with monometallic Pt, is at least partially resulting from a reduced O-poisoning effect due to the weaker metal−O bond on the bimetallic surface. Our DFT results in Figure 1 are consistent with this argument, as indicated by the weaker metal−O binding energy on Pt−Co−Pt than that on Pt. At the same time, the DFT results in Figure 1 also indicate that the binding energy of atomic oxygen is significantly higher on the Co−Pt−Pt surface than on Pt. Using the same O-poisoning argument, one would predict that the Co−Pt−Pt surface should have lower ORR activity than pure Pt due to the stronger bond between surface metal and O atoms. Therefore, the gradual structural transformation of Pt−Co−Pt to Co−Pt−Pt, which should occur in the oxygen-containing cathode environment, could at least partially account for the deactivation of the Co/Pt bimetallic cathode electrocatalysts in the ORR reactions. Furthermore, the DFT results in Figure 1 predict that all other Pt−3d bimetallic alloys should undergo similar structural transformation, from Pt−3d−Pt to 3d−Pt−Pt, leading to a gradual reduction of the ORR activity due to the stronger O−metal bonds on the 3d−Pt−Pt surfaces.

On the basis of the results from the current study, there are two possible solutions to design Pt-based bimetallic catalysts that would have higher ORR activity while retaining the stability in the cathode environment. The first one is to identify Pt−M−Pt bimetallic systems that bond to atomic oxygen more weakly than Pt, at the same time with the O/Pt−M−Pt subsurface structure being thermodynamically more stable than the O/M−Pt−Pt surface structure. We are currently performing

DFT calculations of binary and ternary alloys to search for such a system. The second possible solution is to identify bimetallic systems with comparable rates of outward segregation and inward diffusion of the subsurface atoms, which would maintain a portion of catalyst surfaces in the Pt−M−Pt structure under the ORR reaction environment. Our results suggest that the Pt−Co system might have such properties, as discussed below.

5.2. Outward Segregation and Inward Diffusion in Pt−Co−Pt and Pt−Ni−Pt. It is important to point out that, in the temperature ranges examined, both the inward diffusion and the oxygen-induced segregation of 3d metals are occurring for the Pt−Co−Pt and Pt−Ni−Pt subsurface structures. From the AES results in Figure 4, the inward diffusion of Co is much more extensive than that of Ni at similar temperatures. For example, the results in Figure 4b show that substantial Co diffusion, in the absence of oxygen, already occurs by 400 K. Furthermore, for the O/Pt−Co−Pt(111) surface, the E_a value for Co segregation is lower at 400−475 K (∼3 kcal/mol) than that at 300−350 K (7 ± 1 kcal/mol), suggesting that the experimentally determined E_a is most likely the difference between the activation barriers of Co outward segregation and inward diffusion. In comparison, the inward diffusion of Ni is relatively insignificant at temperatures below 500 K, which is most likely responsible for the higher apparent activation barrier for Ni segregation (15 ± 2 kcal/mol). The relative ease of Co segregation and diffusion suggests the possibility of maintaining at least a fraction of the Pt−Co−Pt subsurface structure under the cathode conditions, which might be responsible for the reported enhancement in both the ORR activity and stability of the Pt−Co bimetallic electrocatalysts in the literature.[1] Additional DFT modeling and AES experiments are underway in our group to quantify the segregation and diffusion of subsurface Co atoms under ORR conditions.

6. Conclusions

From the results and discussion presented above, the following conclusions can be made regarding the stability of Pt−3d alloy surfaces in the presence of oxygen:

(1) The DFT results indicate that, in the presence of adsorbed oxygen, the Pt−3d−Pt subsurface structure is no longer thermodynamically stable. The stable surface structure is the one with 3d metals on the topmost surface, 3d−Pt−Pt, leading to a thermodynamic driving force for the segregation of subsurface 3d atoms. These results are different from the stability of clean and H-covered Pt−3d alloys, where the Pt−3d−Pt subsurface structure is more stable than 3d−Pt−Pt.

(2) The DFT results suggest that desirable Pt−M−Pt bimetallic ORR catalysts should have weaker metal−O binding energy while maintaining the Pt−M−Pt subsurface structure in the presence of oxygen. The latter can be achieved by identifying Pt−M−Pt systems with either higher thermodynamic stability or higher apparent activation barrier for the segregation of the subsurface metal atoms.

(3) The segregation of subsurface Co and Ni to the surfaces of the Pt−3d−Pt structure has been confirmed experimentally using AES and HREELS. The apparent activation energy for the segregation is 7 ± 1 kcal/mol for Co and 15 ± 2 kcal/mol for Ni. AES results also suggest that the outward segregation and inward diffusion of Co atoms are coexistent in the Co/Pt surfaces, which should maintain some Pt−Co−Pt subsurface structures that are more active than Pt for ORR in the oxygen-containing cathode environment.

Acknowledgment. We acknowledge financial support from the Basic Energy Sciences of the Department of Energy (DOE/BES Grant No. DE-FG02-00ER15104). We also acknowledge partial financial support from W.L. Gore and Associates, Inc. and inputs from Drs. William Johnson, Mahesh Murthy, and Daniel Frydrych.

References and Notes

(1) Toda, T.; Igarashi, H.; Uchida, H.; Watanabe, M. *J. Electrochem. Soc.* **1999**, *146*, 3750−3756.
(2) Mukerjee, S.; Srinivasan, S.; Soriaga, M. P.; Mcbreen, J. *J. Electrochem. Soc.* **1995**, *142*, 1409−1422.
(3) Toda, T.; Igarashi, H.; Watanabe, M. *J. Electroanal. Chem.* **1999**, *460*, 258−262.
(4) Antolini, E.; Salgado, J. R. C.; Gonzalez, E. R. *J. Electroanal. Chem.* **2005**, *580*, 145−154.
(5) Yang, H.; Vogel, W.; Lamy, C.; Alonso-Vante, N. *J. Phys. Chem. B* **2004**, *108*, 11024−11034.
(6) Stamenković, V.; Schmidt, T. J.; Ross, P. N.; Marković, N. M. *J. Electroanal. Chem.* **2003**, *554*, 191−199.
(7) Paulus, U. A.; Wokaun, A.; Scherer, G. G.; Schmidt, T. J.; Stamenković, V.; Markovic, N. M.; Ross, P. N. *Electrochim. Acta* **2002**, *47*, 3787−3798.
(8) Stamenković, V.; Schmidt, T. J.; Ross, P. N.; Marković, N. M. *J. Phys. Chem. B* **2002**, *106*, 11970−11979.
(9) Balbuena, P. B.; Altomare, D.; Vadlamani, N.; Bingi, S.; Agapito, L. A.; Seminario, J. M. *J. Phys. Chem. A* **2004**, *108*, 6378−6384.
(10) Anderson, A. B.; Roques, J.; Mukerjee, S.; Murthi, V. S.; Marković, N. M.; Stamenković, V. *J. Phys. Chem. B* **2005**, *109*, 1198−1203.
(11) Xu, Y.; Ruban, A. V.; Mavrikakis, M. *J. Am. Chem. Soc.* **2004**, *126*, 4717−4725.
(12) Zhang, J. L.; Vukmirovic, M. B.; Xu, Y.; Mavrikakis, M.; Adzic, R. R. *Angew. Chem., Int. Ed.* **2005**, *44*, 2132−2135.
(13) Kitchin, J. R.; Khan, N. A.; Barteau, M. A.; Chen, J. G.; Yakshinksiy, B.; Madey, T. E. *Surf. Sci.* **2003**, *544*, 295−308.
(14) Kitchin, J. R.; Nørskov, J. K.; Barteau, M. A.; Chen, J. G. *Phys. Rev. Lett.* **2004**, *93*, 156801-1−156801-4.
(15) Kitchin, J. R.; Nørskov, J. K.; Barteau, M. A.; Chen, J. G. *J. Chem. Phys.* **2004**, *120*, 10240−10246.
(16) Colón-Mercado, H. R.; Kim, H.; Popov, B. N. *Electrochem. Commun.* **2004**, *6*, 795−799.
(17) Colón-Mercado, H. R.; Popov, B. N. *J. Power Sources* **2005**.
(18) Yu, P.; Pemberton, M.; Plasse, P. *J. Power Sources* **2005**, *144*, 11−20.
(19) Bardi, U.; Atrei, A.; Rovida, G.; Ross, P. N. *Surf. Sci.* **1991**, *251*, 727−730.
(20) Gauthier, Y. *Surf. Rev. Lett.* **1996**, *3*, 1663.
(21) Nieuwenhuys, B. E. *Surf. Rev. Lett.* **1996**, *3*, 1869.
(22) Bardi, U.; Beard, B. C.; Ross, P. N. *J. Vac. Sci. Technol., A* **1988**, *6*, 665−670.
(23) An, K. S.; Kimura, A.; Ono, K.; Kamakura, N.; Kakizaki, A.; Park, C. Y.; Tanaka, K. *Surf. Sci.* **1998**, *401*, 336−343.
(24) An, K. S. *Vacuum* **2003**, *72*, 177−181.
(25) Jacob, T.; Merinov, B. V.; Goddard, W. A. *Chem. Phys. Lett.* **2004**, *385*, 374−377.
(26) Khan, N. A.; Zellner, M. B.; Murillo, L. E.; Chen, J. G. *Catal. Lett.* **2004**, *95*, 1−6.
(27) Khan, N. A.; Murillo, L. E.; Chen, J. G. *J. Phys. Chem. B* **2004**, *108*, 15748−15754.
(28) Frühberger, B.; Chen, J. G. *J. Am. Chem. Soc.* **1996**, *118*, 11599−11609.
(29) *Pseudopotential Library* http://oldwww.fysik.dtu.dk/CAMPOS/Documentation/Dacapo/PseudoPotentialOverView/Pt/PW91/pt_us_gga.pseudo.html.
(30) http://www.fysik.dtu.dk/CAMPOS.
(31) Nørskov, J. K.; Rossmeisl, J.; Logadottir, A.; Lindqvist, L.; Kitchin, J. R.; Bligaard, T.; Jonsson, H. *J. Phys. Chem. B* **2004**, *108*, 17886−17892.
(32) Frühberger, B.; Eng, J.; Chen, J. G. *Catal. Lett.* **1997**, *45*, 85−92.
(33) Gland, J. L.; Sexton, B. A.; Fisher, G. B. *Surf. Sci.* **1980**, *95*, 587−602.
(34) Parker, D. H.; Bartram, M. E.; Koel, B. E. *Surf. Sci.* **1989**, *217*, 489−510.
(35) Gland, J. L.; Kollin, E. B. *J. Chem. Phys.* **1983**, *78*, 963−974.
(36) Chen, J. G.; Weisel, M. D.; Hall, R. B. *Surf. Sci.* **1991**, *250*, 159−168.
(37) Rahman, T. S.; Mills, D. L.; Black, J. E.; Szeftel, J. M.; Lehwald, S.; Ibach, H. *Phys. Rev. B* **1984**, *30*, 589−603.
(38) Schwarz, E.; Ernst, K. H.; Gonserbuntrock, C.; Neuber, M.; Christmann, K. *Vacuum* **1990**, *41*, 180−184.
(39) Zellner, M. B.; Goda, A. M.; Skoplyak, O.; Barteau, M. A.; Chen, J. G. *Surf. Sci.* **2005**, *583*, 281−296.
(40) Liu, P.; Rodriguez, J. A.; Muckerman, J. T.; Hrbek, J. *Phys. Rev. B* **2003**, *67*, 155416.